ChemPubSoc Europe

DOI: 10.1002/celc.201600078

CHEMELECTROCHEM
Communications

Two-Step Oxidation of Mxene in the Synthesis of Layer-Stacked Anatase Titania with Enhanced Lithium-Storage Performance

Huang Tang,[a] Shihao Zhuang,[a] Zhihao Bao,*[a] Changshi Lao,[b] and Yongfeng Mei*[c]

Layer-stacked anatase titania (a-TiO_2) was synthesized with two-step oxidation of MXene ($Ti_3C_2T_x$, T = O, OH, or F). Compared with direct oxidation of MXene in air, the two-step oxidation process involving additional hydrothermal pre-oxidation could alleviate the anomalous grain growth of TiO_2, and largely keep the fine structure of MXene. The layered structure derived from MXene enabled the synthesized a-TiO_2 to exhibit superior electrochemical properties. Its discharge capacities reached 241.9 and 131.1 $mA\,h\,g^{-1}$ at the current rates of 0.3 and 12 C, respectively. Even after 10 000 cycles at 6 C, its capacity remained at 107.1 $mA\,h\,g^{-1}$, which is approximately 70 % of the initial capacity. Cyclic voltammetry analysis showed that both diffusive lithium storage in the bulk and interfacial (pseudocapacitive) lithium storage at the surface of layer-stacked a-TiO_2 contributed to its electrochemical properties.

1. Introduction

As the energy and environment crisis becomes increasingly severe, it is important to develop storage devices [e.g. lithium ion batteries (LIBs)] for sustainable and clean energy. One of the challenges for developing LIBs is to design and produce environmentally friendly electrode materials with high capacity and long-term cycle stability.[1,2] Anatase titania (a-TiO_2), as such a candidate anode material, attracts a lot of attention.[3,4] However, a-TiO_2 exhibits particle-size-dependent electrochemistry. The reduction of the a-TiO_2 size can improve its storage capacity and rate capabilities, owing to the short path lengths for lithium diffusion and electronic transport.[5,6] Thus, a-TiO_2 with various nanostructures such as quantum dots,[7] nanosheets,[8] nanotubes,[9,10] and nanospheres[11–13] have been studied for LIB applications. However, few researches have reported a-TiO_2 with a layered nanostructure and its corresponding electrochemical performance. Recently, two-dimensional, exfoliated transition-metal carbides and carbonitrides (MXenes) have been synthesized by selective etching of the A element in HF acid from an MAX phase (e.g. Ti_3AlC_2 and Ti_3AlCN).[14–17] As electrode materials for supercapacitors, some MXenes exhibit high volumetric capacitances with high rate capabilities, partially owing to their layer-stacked nanostructure.[18–20] On the contrary, some features of MXenes might be detrimental to their performance as anodes for LIB applications.[21] For example, ample functional groups (e.g. −OH and −F) and other defects on the surface of MXenes might cause irreversible lithium storage, decreasing their coulombic efficiency. Meanwhile, un-equivalent lithium-ion insertion/extraction sites exist in MXenes with low crystallinity, causing the absence of a charge/discharge plateau. Overall, MXenes do not exhibit exceptional performance as anode materials for LIB applications. To maintain the layered structure of MXenes while converting them to their corresponding oxides (e.g. TiO_2), with improved crystallinity, we herein reported a two-step oxidation process of MXenes ($Ti_3C_2T_x$, T = O, OH, or F surface-terminated group). The process involves pre-oxidation with a hydrothermal reaction and subsequent oxidation in air at 300 °C. This can alleviate the anomalous grain growth of a-TiO_2, which occurs in the direct oxidation of $Ti_3C_2T_x$ in air.[22] The a-TiO_2 with a layered structure inherited from the MXene exhibits superior electrochemical properties. The discharge capacities reach 241.9 and 131.1 $mA\,h\,g^{-1}$ at current rates of 0.3 and 12 C, respectively (1 C = 167.5 $mA\,h\,g^{-1}$). Even after 10 000 cycles at 6 C, the capacity remained at 107.1 $mA\,h\,g^{-1}$, which is about 70 % of the initial capacity.

2. Results and Discussion

The synthesis process for layer-stacked a-TiO_2 is illustrated in Figure 1. In the process, Ti_3AlC_2 was synthesized by keeping a Ti_2AlC–TiC mixture at 1350 °C for 2 h.[14] The X-ray diffraction (XRD) pattern of Ti_3AlC_2 is shown in Figure 2 (black curve); most diffraction peaks could be readily indexed to Ti_3AlC_2 (JCPDS card no. 52-0875) with a small amount of unreacted Ti_2AlC and TiC. After the synthesized Ti_3AlC_2 powders were immersed in HF solution, Al layers were selectively etched away from Ti_3AlC_2 and replaced by O, OH, or F.[14,16] The formed product, MXene ($Ti_3C_2T_x$, T = O, OH, or F), was confirmed according to the XRD pattern (red curve in Figure 2).[14] The scanning

---

[a] Dr. H. Tang, S. Zhuang, Prof. Z. Bao
Shanghai Key Laboratory of Special Artificial Microstructure Materials and Technology, School of Physics Science and Engineering
Tongji University
1239 Siping Road, Shanghai 200092 (China)
E-mail: zbao@tongji.edu.cn

[b] Prof. C. Lao
College of Mechatronics and Control Engineering
Shenzhen University
3688 Nanhai Ave, Shenzhen 518060 (China)

[c] Prof. Y. Mei
Department of Materials Science and Engineering
Fudan University
220 Handan Road, Shanghai 200433 (China)
E-mail: yfm@fudan.edu.cn

Supporting Information for this article can be found under: http://dx.doi.org/10.1002/celc.201600078.

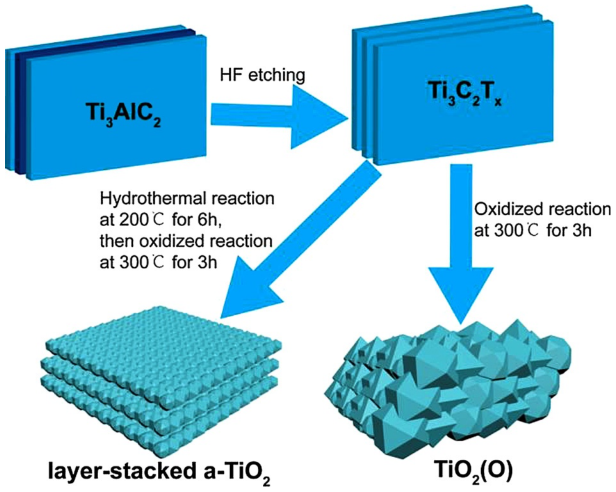

Figure 1. Schematic illustration of the two different oxidation processes of Mxenes.

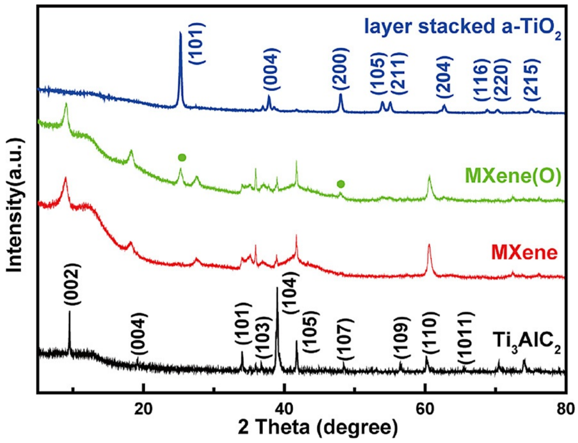

Figure 2. XRD patterns of the Ti_3AlC_2 (black curve), MXene (red curve), MXene(O) (green curve), and layer-stacked anatase TiO_2 (blue curve).

electron microscopy (SEM) images (Figures 3 a and 3 b) show the morphology of the Ti_3AlC_2 particles. After HF etching, MXene exhibited a layer-stacked nanostructure, resembling exfoliated graphite (Figures 3 c and 3 d). After further hydrothermal reaction at 200 °C for 6 h, MXene was partially oxidized into MXene(O) with small amount of a-TiO_2, which was confirmed by the appearance of peaks at 25.28 and 48.05° in the XRD pattern (green curve in Figure 2). Layer-stacked a-TiO_2 was synthesized upon further oxidation of MXene(O) at 300 °C for 3 h in air. The XRD pattern (blue curve in Figure 2) of the product confirmed that it was a-TiO_2 without impurities. Its morphology retained the layer-stacked structure, even though the layer was observed to be composed of titania nanoparticles with sizes of approximately 10 nm (Figures 3 e and 3 f). The TEM image (Figure 4 a) shows a two-dimensional stacking multilayer structure. Under high-resolution (Figure 4 b), a clear lattice spacing of 0.35 nm was observed, which corresponds to the (101) plane of a-TiO_2. As a comparison, MXene was also directly oxidized in air at 300 °C for 3 h. The XRD pattern of the product showed sharp titania peaks (Figure S1), indicating a large titania crystallite size. The crystallite size was estimated to be approximately 100 nm from the high-resolution SEM images (Figures 3 g and 3 h). Clearly, the two-step oxidation process suppressed the anomalous crystallite growth of titania compared with direct oxidation in air. It is believed to be related to the formation of carbon during the hydrothermal oxidation of MXene. In fact, the hydrothermal reaction has already been used to develop amorphous carbon or graphite films on silicon carbide fibers as silicon oxide was formed.[23] It was further proven by the thermogravimetric analysis (TGA), as shown in Figure S2 a. The mass of MXene(O) firstly decreased, owing to the loss of the hydroxyl and fluorine functional groups

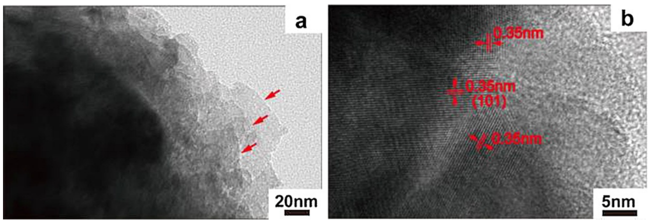

Figure 4. TEM image (a) and HRTEM image (b) of layer-stacked anatase TiO_2.

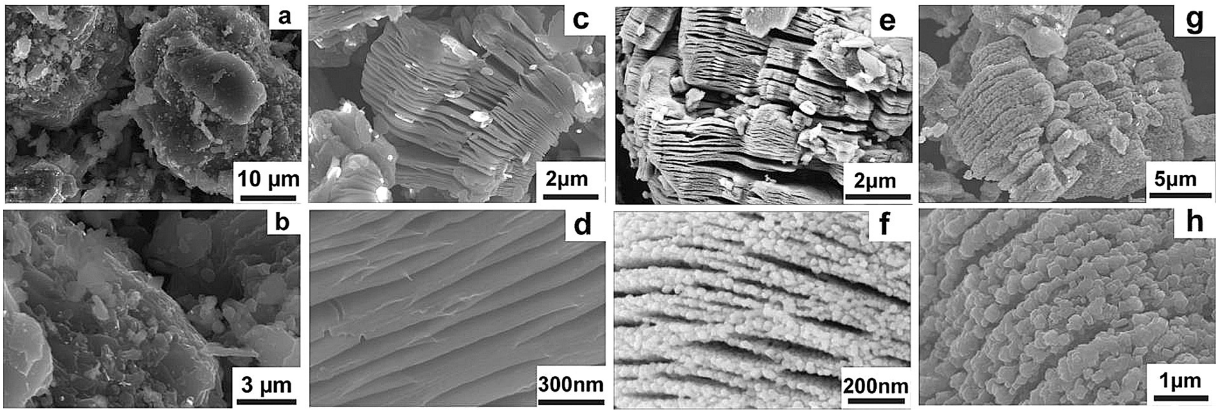

Figure 3. SEM images of Ti_3AlC_2 (a, b), MXene (c, d), layer-stacked anatase TiO_2 (e, f), and TiO_2(O) (g, h).

below 200 °C. Then, the mass increased, because of the oxidation of MXene(O). The overall weight loss was 5.3 %, which could be attributed to the loss of amorphous carbon. On the other hand, the mass of layer-stacked a-TiO_2 remained unchanged when the temperature was below 400 °C, which indicated that almost no functional groups existed in the a-TiO_2. When the temperature was further raised to 800 °C, the mass of a-TiO_2 only lost 1.1 wt % during the calcination, indicating that the layer-stacked a-TiO_2 contained a small amount of carbon. The appearance of carbon was also confirmed by Raman spectra (Figure S2 b). There were two peaks at 1350 and 1580 cm^{-1}, corresponding to the D and G bands of carbon, respectively.[24] In addition, the Raman spectrum of layer-stacked a-TiO_2 showed a strong peak at about 150 cm^{-1} together with three other peaks at about 203, 399, and 629 cm^{-1}, which could be assigned to the $E_{g(1)}$, $E_{g(2)}$, $B_{1g(1)}$, and $E_{g(3)}$ vibrational modes of a-TiO_2, respectively.[25] The amorphous carbon or graphite species formed during the hydrothermal process could somehow hinder mass diffusion through the crystal boundary of MXene(O) during oxidation in air.

To evaluate the electrochemical performance of layer-stacked a-TiO_2, the samples were used as the anode material for a LIB. Figure 5 a shows the galvanostatic charge and discharge profiles at a current density of 0.05 $A\,g^{-1}$ (0.3 C). After the first cycle, the following cycles become stable, and the discharge curve could be divided into three different voltage regions.[4] In region 1, a monotonic voltage drop from 2.80 to 1.74 V corresponded to the storage of approximately 0.12 mol Li per mole TiO_2, which is common and can be linked to the decrease in particle and crystallite sizes of the nanomaterials.[4,26] The second region, a typical biphase plateau, was observed at a potential of about 1.74 V, where a Li-rich phase (Li_xTiO_2) is expected to coexist with a Li-poor phase (a-TiO_2). Upon further Li insertion, the third region with a slope appeared. It was a typical capacitive discharge region for a-TiO_2. The slope of the region could be correlated with the particle size, that is, the shallower the slope, the smaller the particle size.[27] In the first discharge cycle, the capacity reached 339.3 $mA\,h\,g^{-1}$, which involved irreversible consumption of lithium because of the defects, and, at the second discharge, the capacity remained at 255.6 $mAh\,g^{-1}$, which is much higher than the typical capacity (167.5 $mA\,h\,g^{-1}$) of a-TiO_2. In general, the lithium-ion insertion/extraction reaction in a-TiO_2 proceeds according to Equation (1):[28]

$$TiO_2 + x\,Li^+ + x\,e^- \rightarrow Li_xTiO_2 \qquad (1)$$

where x is the lithium insertion coefficient. For anatase, $x = 0.5$ corresponds to the phase transformation from tetragonal TiO_2 to orthorhombic $Li_{0.5}TiO_2$. In this transformation, the theoretical capacity was calculated to be 167.5 $mA\,h\,g^{-1}$.[29] Meanwhile, the crystal particle size emerged as an effective parameter to promote the solubility and solid solution behavior, as well as alter insertion capacities.[5] Figure 5 b shows the rate capability of layer-stacked a-TiO_2. Its discharge capacities were 241.9, 216.2, 199.1, 172.6, 151.5, and 131.1 $mA\,h\,g^{-1}$ at current rates of 0.3, 0.6, 1.2, 3, 6, and 12 C, respectively. When the current rate returned to 0.6 C, the capacity increased back to 212.0 $mA\,h\,g^{-1}$, which was almost 98.1 % of the initial capacity at 0.6 C. In contrast, the TiO_2(O) sample from the one-step oxidation reaction, showed poor performance and only maintained 116.4 $mA\,h\,g^{-1}$

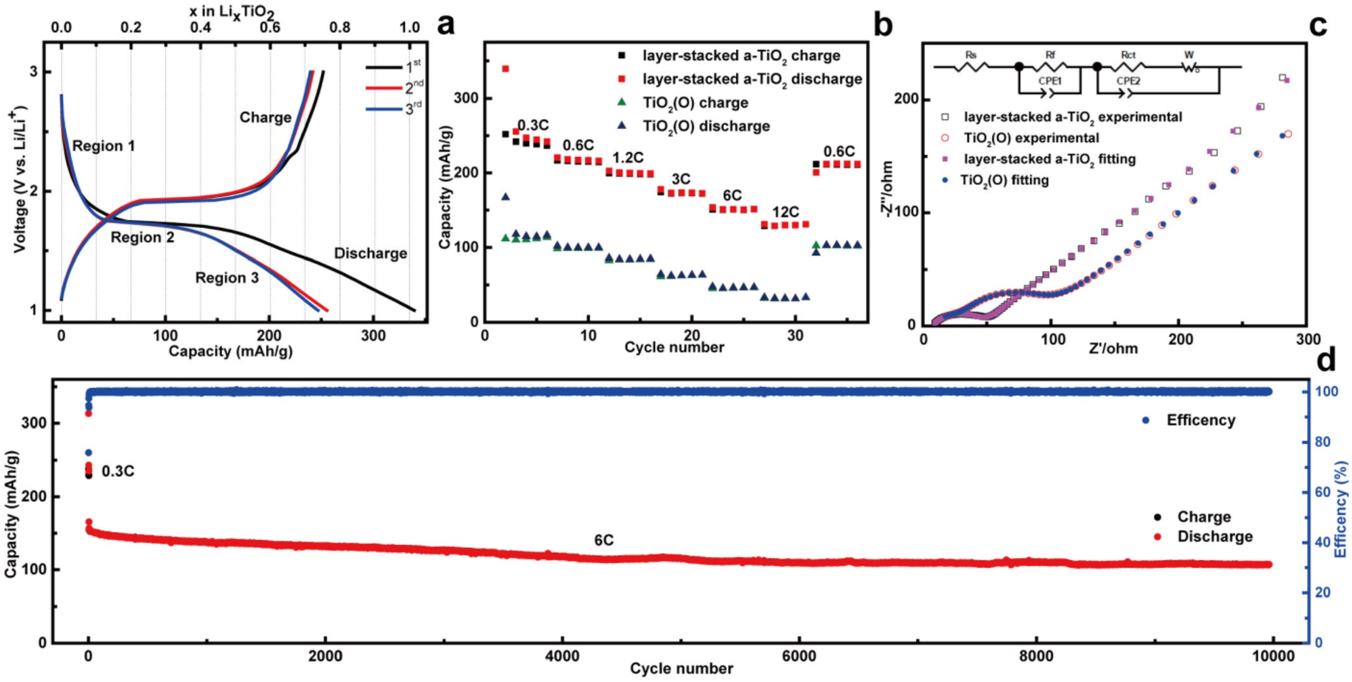

Figure 5. Electrochemical performance of TiO_2 electrodes. a) Galvanostatic charge and discharge profiles for layer-stacked anatase TiO_2 at a current density of 0.05 $A\,g^{-1}$. b) Rate performance of layer-stacked anatase TiO_2 and TiO_2(O) at different current rates. c) Nyquist plots of layer-stacked anatase TiO_2 and TiO_2(O) (inset: equivalent circuit). d) Long-term cycling performance of layer-stacked anatase TiO_2 at a high current rate of 6 C.

at 0.3 C and 33.3 mA h g^{-1} at 12 C. Electrochemical impedance spectroscopy (EIS) measurements are shown in Figure 5 c. Both Nyquist plots consist of one depressed semicircle at high–medium frequency and a linear section in the low-frequency region. The EIS data were analyzed based on the equivalent circuit inset in Figure 5 c. The depressed semicircle is composed of two standard semicircles based on the fitting of the Nyquist plots. The diameter of the first semicircle at high frequency relates to the surface layer resistance R_f, which can be ascribed to lithium-ion diffusion through the surface layer, and the diameter of the second semicircle at medium frequency relates to the charge-transfer resistance R_{ct}.[30] As shown in Table S1, the R_f and R_{ct} values for the layer-stacked a-TiO_2 electrode were lower than those of the TiO_2(O) electrode, which could be attributed to straightforward contact between the layer structure and electrolyte for better electron and Li^+ transport. To test the cycle stability of layer-stacked a-TiO_2, the electrode was discharged/charged at 6 C (1 A g^{-1}) for 10 000 cycles after aging at 0.3 C for three cycles (Figure 5 d). The reversible capacities were 154.2, 147.6, 137.7, and 107.1 mA h g^{-1} in the 10th, 100th, 1000th, and 10 000th cycle, respectively. The capacity in the 10 000th cycle was about 70 % of the capacity in the 10th cycle; the calculated coulombic efficiency was about 99.996 %, which indicated superior long-term, high-rate, and completely reversible lithium-storage capabilities. The capacity was superior to most anatase TiO_2 species previously reported, which have been summarized in Table S2. Such a superior performance could be attributed to its unique morphology. Firstly, the layer structure composed of TiO_2 nanoparticles (ca. 10 nm) led to better interstitial dynamics and a short diffusion path in Li-ion storage.[5] Secondly, the layer structure was able to be embedded with a conductive agent (i.e. super P) and facilitated Li^+ transport during the lithium insertion/extraction process. Meanwhile, the space between the layers could accommodate the stress that occurs during insertion/extraction, maintaining the structure of the materials; the SEM image of the electrode after the first lithiation is shown in the Figure S3 b. Moreover, the layer-structure morphology was well retained after long-term cycling (e.g. 1000 cycles), which was confirmed by the SEM image shown in Figure S3 c. As a comparison, the electrochemical performance of commercial anatase TiO_2 (com-TiO_2, Aladdin, 60 nm) is shown in Figure S4. It exhibits a poor rate capability and fast capacity fading with cycling. For $Ti_3C_2T_x$, there was no voltage plateau in its galvanostatic charge/discharge curve (Figure S5) with low coulombic efficiency, which can partially be ascribed to the ample functional groups such as fluorine, or possibly hydroxyls, on its surface.[21] The reported electrochemical performance of MXenes is also summarized in Table S3. Compared with com-TiO_2 and MXenes, layer-stacked a-TiO_2 exhibits an increased specific capacity and enhanced rate capability, owing to its layer-crystallized structure.

To explore the lithium-storage mechanism, cyclic voltammograms (CVs) were analyzed. Figure 6 a shows the CVs obtained at different scan rates from 0.1 to 5 mV s^{-1} in a voltage range between 1.0 and 3.0 V for layer-stacked a-TiO_2. One pair of distinct cathodic (insertion)/anodic (extraction) peaks could be observed at each scan rate. The cathodic/anodic peaks were located at 1.73 and 2.03 V, respectively, at a scan rate of 0.1 mV s^{-1}, corresponding to the voltage plateaus obtained from the galvanostatic cycling. The cathodic peak current was almost equal to the anodic peak current, indicating that the insertion/extraction of Li ions in layer-stacked a-TiO_2 nanoparticles was highly reversible.[31] The total stored charge mainly consists of two components: the faradaic contribution from the Li-ion insertion process, and the pseudocapacitive effect in the charge-transfer process with surface atoms.[27] The capacitive effects were investigated by analyzing the cyclic voltammetry data at various rate following the power law [Eq. (2)]:[32]

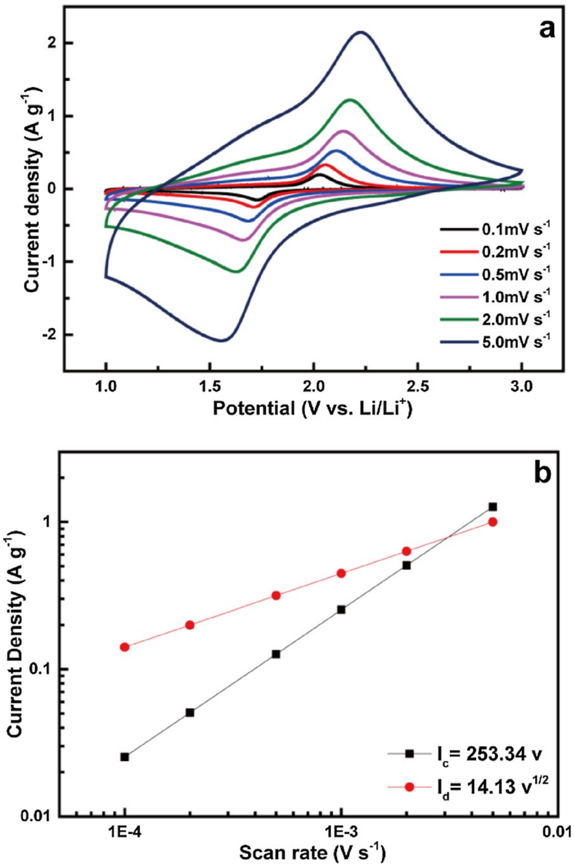

Figure 6. a) CVs of layer-stacked anatase TiO_2 at various scan rates. b) Calculated surface pseudocapacitive (I_c) and bulk insertion (I_d) discharge currents.

$$I_p = av^b \qquad (2)$$

where I_p is the peak discharge current, v the scan rate, and a and b are adjustable parameters. There were two well-defined conditions, when $b = 0.5$, the peak current was proportional to the square root of the scan rate, indicating a Li-ion insertion process; when $b = 1.0$, the peak current had a linear relationship with scan rate, corresponding to current contributions from the pseudocapacitive effect.[27] Figure S6 shows the linear relationship between $\log I_p$ and $\log v$ for layer-stacked a-TiO_2, The power law relationship was $I_p \propto v^{0.665}$, exhibiting a mixture between the diffusion-limited ($I_p \propto v^{0.5}$) and capacitive behavior ($I_p \propto v$), as discussed above.[32] The mixed lithium-storage process can be expressed as Equation (3):[33]

$$I_p = C_1 v + C_2 v^{1/2} \quad (3)$$

where $I_c = C_1 v$ represents the current contributions from the surface capacitive effects and $I_d = C_2 v^{1/2}$ corresponds to the lithium-insertion process. To facilitate the analysis, Equation (3) can be rewritten the following format [Eq. (4)]:

$$I_p / v^{1/2} = C_1 v^{1/2} + C_2 \quad (4)$$

C_1 and C_2 were determined to be 253.34 and 14.13 from Figure 6a, respectively. Figure 6b shows the relationship between I_c and I_d at various scan rates. At a low scan rate of 0.1 mV s^{-1}, the I_c was much smaller than I_d, indicating that the lithium-insertion process dominated the whole storage mechanism. As the scan rate increased, both I_c and I_d increased. When the scan rate exceeded 3 mV s^{-1}, I_c became larger than I_d, which indicated that the pseudocapacitive storage predominated at a high scan rate. The above results indicated both bulk lithium-storage and interfacial lithium-storage mechanisms contributed its overall electrochemical performance.

3. Conclusions

Layer-stacked a-TiO_2 was successfully synthesized through the two-step oxidation of MXene. The two-step oxidation process could alleviate the anomalous grain growth of TiO_2, and largely kept the fine layer structure of MXene. Each layer was composed of approximately 10 nm necked a-TiO_2 nanoparticles. Such a layered structure enabled the synthesized titania to exhibit long-term, high-rate, and almost completely reversible lithium-storage capabilities. The a-TiO_2 discharge capacities reached 241.9 and 131.1 mA h g^{-1} at current rates of 0.3 and 12 C, respectively. After 10 000 cycles at 6 C, the capacity maintained approximately 70 % of the initial capacity. Both bulk lithium storage and pseudocapacitive contributed to the overall storage capabilities.

Experimental Section

Synthesis of Ti_3AlC_2

To synthesize Ti_3AlC_2, commercially available Ti_2AlC (>92 %, 325 mesh) and TiC (>99 %, 2000 mesh) were mixed in an argon environment by using agate balls on a planetary rotator at 300 revolutions per minute in a 1:1 molar ratio for 12 h; the diameters of agate balls were 10 mm for three balls and 6 mm for five balls. The XRD spectra of the raw materials are shown in Figure S7. Then, the mixture was heated to 1350 °C with a rate of 5 °C min^{-1} and kept at that temperature for 2 h under an argon flow. The resulting product was ground in the agate mortar, and sieved (325 mesh) prior to use.[14]

Synthesis of MXene ($Ti_3C_2T_x$)

Ti_3AlC_2 (3 g) was immersed in HF solution (30 mL; 50 wt %, Aladdin) in a polytetrafluoroethylene jar with magnetic stirring for 48 h; the molar ratio of Ti_3AlC_2 to HF was about 1:60. Then, the resulting suspension was washed several times with centrifugation, until the pH reached around 6.0. The product was finally vacuum dried at 50 °C for 12 h to obtain $Ti_3C_2T_x$.

Synthesis of Layer-Stacked a-TiO_2

MXene ($Ti_3C_2T_x$; 100 mg) was added to deionized water (20 mL). It was then transferred to a 25 mL autoclave and kept at 200 °C for 6 h. The resulting precipitate was cleaned several times by using deionized water with centrifugation. The product [labeled MXene(O)] was vacuum dried at 50 °C. It was further oxidized at 300 °C for 3 h in air to obtain layer-stacked a-TiO_2. For comparison, MXene was heated to 300 °C and maintained at the temperature for 3 h in air. The above product was labeled TiO_2(O).

Material Characterization

XRD patterns were obtained by using a diffractometer (Bruker D8 Advance) with Cu K$_\alpha$ radiation (λ = 1.5418 Å, 40 kV, 40 mA). Raman spectra were measured on a Labram HR-800 spectrometer with a 514 nm laser beam. The carbon content in TiO_2 was determined by using a thermogravimetry instrument (PerkinElmer Pyris 1 TGA), and the measurements were carried out in air in a range of 25–800 °C with a ramp rate of 10 °C min^{-1}. The morphology and microstructure of samples were observed by using field-emission scanning electron microscopy (FESEM, Zeiss Ultra55) and high-resolution transmission electron microscopy (HRTEM, JEOL 2100F).

Electrochemical Measurements

The powder of a-TiO_2 as the active material, Super P carbon black, and polyvinyldifluoride (weight ratio 70:20:10) were mixed in *N*-methylpyrrolidone solvent to produce a slurry. The slurry was coated onto a copper foil by using the doctor-blading method and then dried to form the working electrode. The electrochemical tests were performed by using two-electrode coin-type cells (CR 2016) with lithium foils as the counter electrode. A 1 M solution of $LiPF_6$ in a 1:1:1 (volume ratio) mixture of ethylene carbonate, diethyl carbonate, and dimethyl carbonate was used as the electrolyte. Cell assembly was carried out in an argon-filled glove box. The mass of active materials loaded onto each electrode was about 1.0 mg. Galvanostatic charge/discharge cycling was conducted by using a battery tester (Land2100A) with a voltage window of 1.0–3.0 V (vs. Li/Li^+) at various current densities. All galvanostatic charge/discharge cycling tests were performed at 25 °C. Cyclic voltammetry tests were performed at different scanning rates from 0.1 to 5 mV s^{-1} between 1.0 and 3.0 V (vs. Li/Li^+) after the initial ten charge/discharge cycles. EIS was conducted in a frequency range from 100 kHz to 10 mHz. Cyclic voltammetry and EIS were performed with an Autolab 302N electrochemical workstation.

Acknowledgements

This work was supported by the Scientific Research Foundation for Returned Scholars, the Ministry of Education of China, Key Basic Research Projects of Science and Technology Commission *of Shanghai (no. 11JC1412900), and the National Science Foundation of China program (no. 21271140, 51472182). The project is also supported by the Fundamental Research Funds for the Central Universities.*

Keywords: anatase titania · electrode materials · layer-stacked nanostructures · lithium-ion batteries · oxidation

[1] J. M. Tarascon, M. Armand, *Nature* **2001**, *414*, 359.
[2] V. Etacheri, R. Marom, R. Elazari, G. Salitra, D. Aurbach, *Energy Environ. Sci.* **2011**, *4*, 3243.
[3] L. Kavan, M. Gratzel, S. E. Gilbert, C. Klemenz, H. J. Scheel, *J. Am. Chem. Soc.* **1996**, *118*, 6716.
[4] Y. G. Guo, Y. S. Hu, J. Maier, *Chem. Commun.* **2006**, 2783.
[5] M. Wagemaker, W. J. H. Borghols, F. M. Mulder, *J. Am. Chem. Soc.* **2007**, *129*, 4323.
[6] C. Jiang, M. Wei, Z. Qi, T. Kudo, I. Honma, H. Zhou, *J. Power Sources* **2007**, *166*, 239.
[7] R. Mo, Z. Lei, K. Sun, D. Rooney, *Adv. Mater.* **2014**, *26*, 2084.
[8] B. Hao, Y. Yan, X. Wang, G. Chen, *ACS Appl. Mater. Interfaces* **2013**, *5*, 6285.
[9] Y. Tang, Y. Zhang, J. Deng, J. Wei, H. L. Tam, B. K. Chandran, Z. Dong, Z. Chen, X. Chen, *Adv. Mater.* **2014**, *26*, 6111.
[10] H.-T. Fang, M. Liu, D.-W. Wang, T. Sun, D.-S. Guan, F. Li, J. Zhou, T.-K. Sham, H.-M. Cheng, *Nanotechnology* **2009**, *20*, 225701.
[11] S. K. Das, S. Darmakolla, A. J. Bhattacharyya, *J. Mater. Chem.* **2010**, *20*, 1600.
[12] N. Li, G. Liu, C. Zhen, F. Li, L. Zhang, H. M. Cheng, *Adv. Funct. Mater.* **2011**, *21*, 1717.
[13] G. Zhang, H. B. Wu, T. Song, U. Paik, X. W. Lou, *Angew. Chem. Int. Ed.* **2014**, *53*, 12590; *Angew. Chem.* **2014**, *126*, 12798.
[14] M. Naguib, M. Kurtoglu, V. Presser, J. Lu, J. Niu, M. Heon, L. Hultman, Y. Gogotsi, M. W. Barsoum, *Adv. Mater.* **2011**, *23*, 4248.
[15] M. Naguib, O. Mashtalir, J. Carle, V. Presser, J. Lu, L. Hultman, Y. Gogotsi, M. W. Barsoum, *ACS Nano* **2012**, *6*, 1322.
[16] M. Naguib, V. N. Mochalin, M. W. Barsoum, Y. Gogotsi, *Adv. Mater.* **2014**, *26*, 992.
[17] M. Naguib, Y. Gogotsi, *Acc. Chem. Res.* **2015**, *48*, 128.
[18] M. R. Lukatskaya, O. Mashtalir, C. E. Ren, Y. Dall'Agnese, P. Rozier, P. L. Taberna, M. Naguib, P. Simon, M. W. Barsoum, Y. Gogotsi, *Science* **2013**, *341*, 1502.
[19] M.-Q. Zhao, C. E. Ren, Z. Ling, M. R. Lukatskaya, C. Zhang, K. L. Van Aken, M. W. Barsoum, Y. Gogotsi, *Adv. Mater.* **2015**, *27*, 339.
[20] M. Ghidiu, M. R. Lukatskaya, M.-Q. Zhao, Y. Gogotsi, M. W. Barsoum, *Nature* **2014**, *516*, 78.
[21] M. Naguib, J. Come, B. Dyatkin, V. Presser, P.-L. Taberna, P. Simon, M. W. Barsoum, Y. Gogotsi, *Electrochem. Commun.* **2012**, *16*, 61.
[22] M. Naguib, O. Mashtalir, M. R. Lukatskaya, B. Dyatkin, C. Zhang, V. Presser, Y. Gogotsi, M. W. Barsoum, *Chem. Commun.* **2014**, *50*, 7420.
[23] Y. G. Gogotsi, M. Yoshimura, *Nature* **1994**, *367*, 628.
[24] F. Tuinstra, J. L. Koenig, *J. Chem. Phys.* **1970**, *53*, 1126.
[25] V. Swamy, A. Kuznetsov, L. S. Dubrovinsky, R. A. Caruso, D. G. Shchukin, B. C. Muddle, *Phys. Rev. B* **2005**, *71*, 184302.
[26] Y. S. Hu, L. Kienle, Y. G. Guo, J. Maier, *Adv. Mater.* **2006**, *18*, 1421.
[27] J. Wang, J. Polleux, J. Lim, B. Dunn, *J. Phys. Chem. C* **2007**, *111*, 14925.
[28] L. Kavan, M. Gratzel, J. Rathousky, A. Zukal, *J. Electrochem. Soc.* **1996**, *143*, 394.
[29] J.-Y. Shin, D. Samuelis, J. Maier, *Adv. Funct. Mater.* **2011**, *21*, 3464.
[30] S. Yoon, A. Manthiram, *J. Phys. Chem. C* **2011**, *115*, 9410.
[31] Y. Y. Xia, H. Takeshige, H. Noguchi, M. Yoshio, *J. Power Sources* **1995**, *56*, 61.
[32] H. Lindström, S. Södergren, A. Solbrand, H. Rensmo, J. Hjelm, A. Hagfeldt, S.-E. Lindquist, *J. Phys. Chem. B* **1997**, *101*, 7717.
[33] T. C. Liu, W. G. Pell, B. E. Conway, S. L. Roberson, *J. Electrochem. Soc.* **1998**, *145*, 1882.

Manuscript received: March 29, 2016
Accepted Article published: April 1, 2016
Final Article published: April 15, 2016